



OPEN

Comprehensive profiling analysis of the N6-methyladenosine-modified circular RNA transcriptome in cultured cells infected with Marek's disease virus

Aijun Sun^{1,2,6}, Rui Wang^{1,2,6}, Shuaikang Yang^{1,2}, Xiaojing Zhu^{1,2}, Ying Liu^{1,2}, Man Teng^{3,4}, Luping Zheng^{3,4}, Jun Luo^{3,4,5}, Gaiping Zhang^{1,2,3} & Guoqing Zhuang^{1,2}✉

Marek's disease virus (MDV) induces severe immunosuppression and lymphomagenesis in the chicken, its natural host, and results in a condition that investigated the pathogenesis of MDV and have begun to focus on the expression profiling of circular RNAs (circRNAs). However, little is known about how the expression of circRNAs is referred to as Marek's disease. Previous reports have is regulated during MDV replication. Here, we carried out a comprehensive profiling analysis of N6-methyladenosine (m⁶A) modification on the circRNA transcriptome in infected and uninfected chicken embryonic fibroblast (CEF) cells. Methylated RNA immunoprecipitation sequencing (MeRIP-Seq) revealed that m⁶A modification was highly conserved in circRNAs. Comparing to the uninfected group, the number of peaks and conserved motifs were not significantly different in cells that were infected with MDV, although reduced abundance of circRNA m⁶A modifications. However, gene ontology and Kyoto encyclopedia of genes and genomes (KEGG) pathway analyses revealed that the insulin signaling pathway was associated with the regulation of m⁶A modified circRNAs in MDV infection. This is the first report to describe alterations in the transcriptome-wide profiling of m⁶A modified circRNAs in MDV-infected CEF cells.

Marek's disease virus (MDV) causes a fatal disease that is referred to as Marek's disease (MD). This is a disease that is characterized by immunosuppression, neurological disorders, and T-cell lymphoma formation¹⁻³. The genome of MDV is approximately 180 kb in size and includes a unique long region (UL) and a unique short region (US), with reverse repetitive complementary sequences at both ends of the genome, and encoding more than 100 genes^{4,5}. MDV can be classified as serotype 1 (MDV-1), serotype 2 (MDV-2), and serotype 3 (MDV-3). MDV-2 and MDV-3 are non-pathogenic while MDV-1 causes a diverse degree of diseases and tumors once it has infected its natural host⁶. Although progress has been made in terms of analyzing gene function in MDV, the precise mechanisms involved in the pathogenesis of this disease have yet to be determined.

Non-coding RNAs (ncRNAs), including microRNAs (miRNAs), long non-coding RNAs (lncRNAs), and circular RNAs (circRNAs), are known to play important regulatory roles in a range of diseases⁷. CircRNAs are a class of long RNA molecules that are over 200 nucleotides in length and are widely expressed in eukaryotes with a closed ring structure, lacking a 5'-cap structure, and a 3'-poly(A) tail. CircRNAs are formed by exon, intron, and exon-intron sequences, and are mainly located in the cytoplasm for post-transcriptional regulation; in this region, circRNAs are stable and not easily degraded by RNA exonuclease⁸. Some circRNAs have been

¹College of Veterinary Medicine, Henan Agricultural University, Zhengzhou 450002, Henan, People's Republic of China. ²International Joint Research Center of National Animal Immunology, College of Veterinary Medicine, Henan Agricultural University, Zhengzhou 450002, Henan, People's Republic of China. ³Key Laboratory of Animal Immunology, Ministry of Agriculture and Rural Affairs and Henan Provincial Key Laboratory of Animal Immunology, Henan Academy of Agricultural Sciences, Zhengzhou 450002, People's Republic of China. ⁴UK-China Centre of Excellence for Research on Avian Diseases, Henan Academy of Agricultural Sciences, Zhengzhou 450002, People's Republic of China. ⁵College of Animal Science and Technology, Henan University of Science and Technology, Luoyang 471003, People's Republic of China. ⁶These authors contributed equally: Aijun Sun and Rui Wang. ✉email: gqzhuang2008@163.com

found in cell nuclei, thus supporting a potential role in the regulation of transcription⁹. It has been reported that circRNA acts as a sponge to regulate the expression of miRNAs¹⁰. Interestingly, virus infection has been shown to alter the landscape of the circRNAs transcriptome may help the virus to escape immune surveillance. It has been demonstrated that circRNAs are also involved in ALV-J-induced tumorigenesis in susceptible and resistant chickens¹¹. In MD-induced spleen tumors, a total of 2169 circRNAs have been identified; these were derived from exons. When comparing spleen samples from survivors and non-infected chickens, 113 circRNAs were identified to be abnormally expressed. Comprehensive analysis revealed that circRNAs may also participate in tumorigenesis by regulating the regulatory network associated with the immune response^{12,13}. However, we do not yet know how circRNAs are regulated during MDV infection.

Recent studies have identified that RNA modifications can regulate the epigenetic. To date, at least 100 RNA modifications have been reported in biological and pathological activities¹⁴. In eukaryotes, 5'-Cap and 3'-poly(A) tail modifications can play an important role in the regulation of transcription, while the internal modification of messenger RNA (mRNA) is used to maintain stability. The most common internal modifications of mRNA include N⁶-methyladenosine (m⁶A), N¹-methyladenosine (m¹A), and N⁵-methylcytosine (m⁵C)¹⁵. m⁶A is the most common reversible base modification on RNA and can affect transcription, splicing, localization, translation, structure stability, and the post-transcriptional regulation of gene expression. m⁶A modification has also been detected on ncRNAs, such as transfer RNA (tRNA) and ribosomal RNA (rRNA)¹⁶. Many enzymes have been identified in m⁶A modification, including methyltransferase and demethylase. Methyl-transferase, which acts as a writer, is an important catalytic enzyme complex that causes m⁶A methylation of bases on RNA, including components of METTL3, METTL14, WTAP, and KIAA1492, and other unknown proteins¹⁷. The m⁶A demethylase complex contains FTO and ALKBH5 proteins and is referred to as an eraser. FTO was first characterized as a member of the Alkb protein family and was associated with obesity. Subsequently, FTO was confirmed as a very important component of the demethylase complex^{18–20}. In addition, m⁶A-modified mRNA needs a specific RNA binding protein-methylated reading protein, which is known as a reader. A variety of reading proteins have been identified by RNA pull-down assays, including YTH domain protein, nuclear heterogeneous ribosomal protein (hnRNP), and eukaryotic initiation factor (EIF). These reading proteins can specifically bind to the m⁶A methylation region, thus weakening homologous binding to RNA-binding proteins and changing the secondary structure of the RNA to regulate interactions between protein and RNA^{15,21}.

Previous studies of m⁶A modification mainly focused on the maintenance of mRNA stability, mRNA precursor splicing, polyadenylate acidification, mRNA transport, and the initiation of translation. In addition, research has shown that ncRNAs also exhibit a large number of base modification activities after transcription²². It has been shown that abnormal patterns of m⁶A modification are involved in a series of diseases, including tumors and viral infections²³. In this study, we investigated the expression profile of circRNA and comprehensively analyzed the m⁶A modification of circRNAs in MDV-infected CEF cells. We also analyzed the signaling pathways associated with the m⁶A modification of circRNAs and the roles of m⁶A modification in MDV infection.

Materials and methods

Cells and virus. Specific-pathogen free (SPF) eggs were purchased from Boehringer Ingelheim (Beijing, China) and incubated at 37 °C in order to isolate primary chicken embryo fibroblast (CEF) cells²⁴, as described previously. CEF cells were prepared after 9 days of incubation, and were then cultured in Dulbecco's modified essential medium (DMEM) (Solarbio, Beijing, China) containing 5% fetal bovine serum (FBS) (Gibco, CA, USA), 100 U/mL of penicillin and 100 µg/mL of streptomycin at 37 °C with 5% CO₂. Secondary CEF cells were seeded to 80–90% confluency in 75 cm² petri dishes. The cells were then inoculated with 10⁶ plaque formation units (PFU) of Md5 (Passage two). Uninfected CEF cells were used as negative control. Seven days post-infection, CEF cells were harvested when cytopathic effects (CPE) became clearly visible in approximately 70–80% of Md5-infected cells.

RNA isolation. Total RNA was extracted from CEF cells using TRIzol reagent (Invitrogen, Carlsbad, CA, USA). The RNA concentration of each sample was then determined with a NanoDrop ND-1000 (Thermo Fisher Scientific, MA, USA). The quality of the RNAs was subsequently identified by measuring the OD₂₆₀/OD₂₈₀ value, and RNA purity was confirmed by measuring the OD₂₆₀/OD₂₃₀ value. RNA integrity and genomic DNA contamination were measured by denatured agarose gel electrophoresis.

Methylated RNA immunoprecipitation sequencing (MeRIP-Seq). Fragmented RNA was incubated with an anti-m⁶A polyclonal antibody (Synaptic Systems, 202003) in immunoprecipitation (IPP) buffer for 2 h at 4 °C²⁵. The reaction mixture was then immunoprecipitated with protein A magnetic beads (Thermo Fisher, MA, USA) at 4 °C for 2 h. Next, the bound RNA was eluted from the beads with N⁶-methyladenosine antibody in IPP buffer and extracted with TRIzol reagent (Thermo Fisher, MA, USA). The extracted RNA was then prepared with a NEBNext Ultra II Directional RNA Library Prep Kit (NEB, MA, USA). Both the input sample (without immunoprecipitation) and the m⁶A immunoprecipitation samples were subjected to 150 bp paired-end sequencing on an Illumina HiSeq sequencer.

Data analysis. Paired-end reads were acquired from an Illumina HiSeq 4000 sequencer and were quality controlled by Q30. Next, 3' adaptor-trimming and low quality reads were removed by cutadapt software (v1.9.3, <https://github.com/marcelm/cutadapt/>) to obtain high quality clean reads. The reads were then aligned to the reference genome (Gal5; GCA_000002315.3) with Hisat2 software (v2.0.4). Expressed circRNAs were identified using input reads. Methylated sites on the circRNA were then identified by the MeTPeak package in the R environment. The MeTDiff package was used to investigate the differential methylation of circRNAs. The Gene

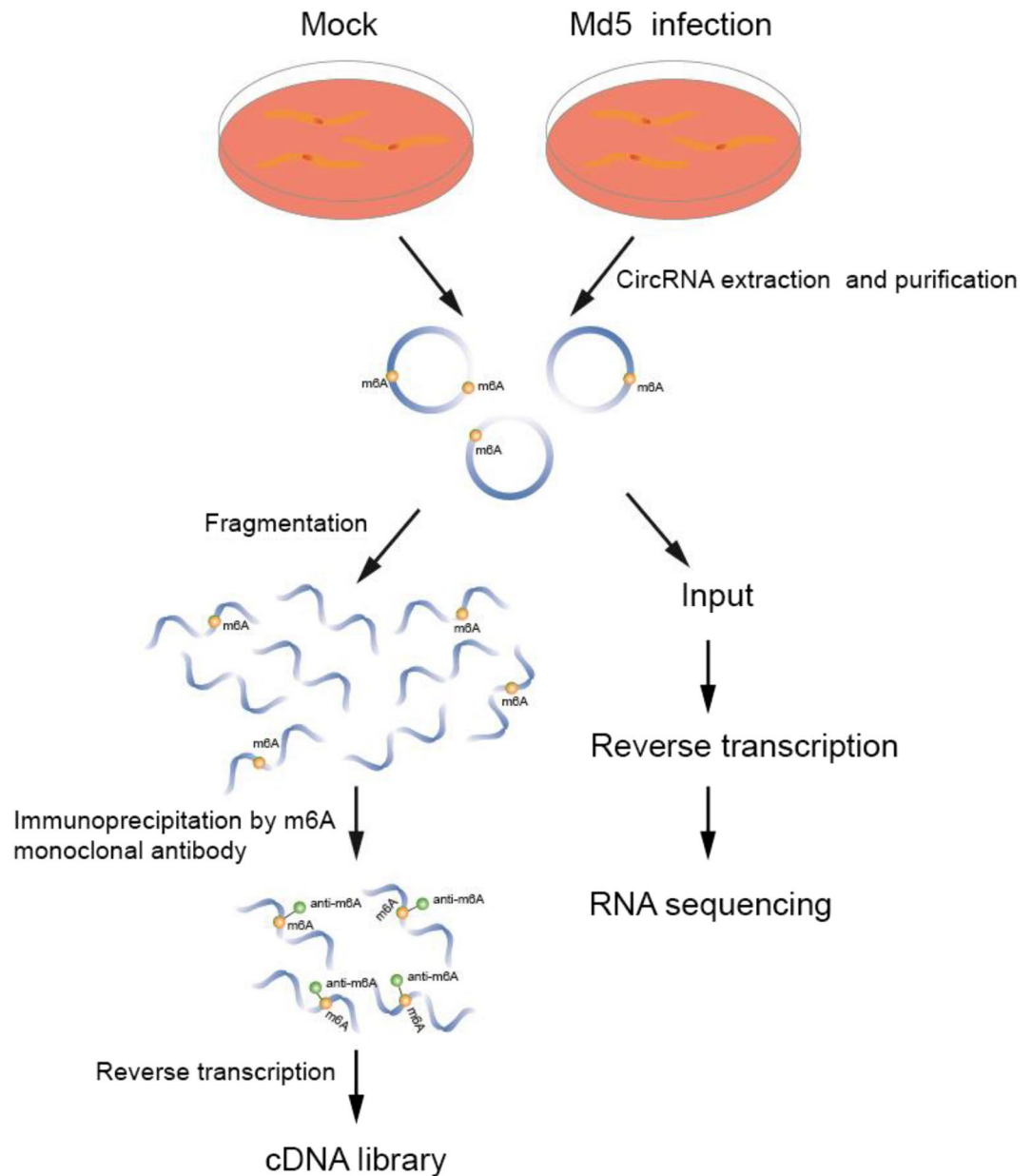


Figure 1. Flowchart depicting construction of cDNA libraries used for m⁶A-modified circRNA transcriptome sequencing of uninfected and Md5-infected CEF cells. (Figure was made by Adobe Illustrator, v 24.0, <https://www.adobe.com/cn/products/illustrator.html>).

Ontology (GO) (<http://www.geneontology.org>) and the Kyoto Encyclopedia of Genes and Genomes (KEGG) (<https://david.ncicrf.gov>) pathway enrichment analyses were performed to identify differentially methylated genes²⁶. The interactive analysis tool Integrative Genomics Viewer (IGV) (v2.4.10, <http://www.igv.org/>) software was used to visualize the alignments on the genome.

Results

Transcriptome-wide analysis of circRNAs in Md5-infected CEF cells. For circRNA transcriptome profiling analysis, we first extracted RNA from the MDV infected group and control group. After RNA fragmentation, RNA were separated into two parts. One was used for regular circRNA transcriptome analysis as input. The other part was enriched by MeRIP-seq assay for m⁶A modified circRNA transcriptome analysis (Fig. 1). A total of 6045 circRNAs, with at least two independent reads, were identified, ranging from 131 nucleotides to 96,080 nucleotides. The circRNAs were derived from exonic, intronic, intergenic, sense overlapping, and antisense regions (Fig. 2A). GO enrichment analysis for biological processes (BP) indicated that genes related to chromosome segregation were up-regulated (Fig. 2B). For molecular functions (MF), genes related to carbohydrate binding were up-regulated, while genes related to glycosaminoglycan binding were down-regulated (Fig. 2C).

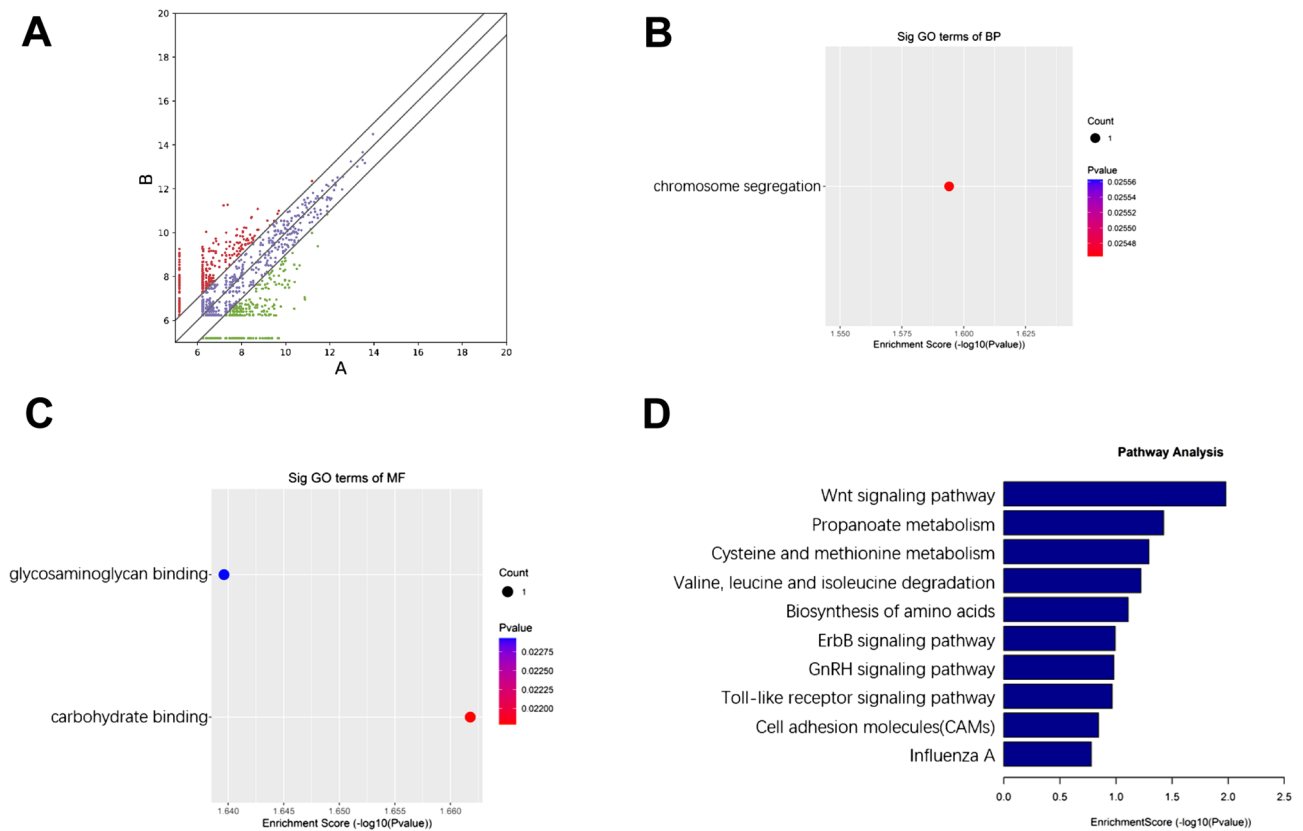


Figure 2. (A) Differentially expressed circRNAs in infected and control groups. The X axis represents the expression level of the gene in the control group, and the Y axis represents the expression level of the gene in the infected group. A represents the uninfected group and B represents the infected group. Red dots represent up-regulated genes in group B compared with group A. Blue dots represent genes with no significant differences in group B compared with group A. (Made by edgeR, v3.16.5, <http://www.bioconductor.org/packages/release/bioc/html/edgeR.html>) (B,C) GO enrichment of host genes associated with down-regulated circRNAs for (B) biological processes and (C) molecular functions; (D) KEGG pathway analysis of the host genes for circRNAs.

For cellular components (CC), no up-regulated or down-regulated genes related to the relevant signaling pathway were detected. We performed KEGG enrichment analysis for the differentially expressed circRNAs, and identified a range of affected pathways, including the Wnt signaling pathway and propanoate metabolism; along with the degradation and metabolism of cysteine, methionine, valine, leucine, and isoleucine. We also identified changes in the biosynthesis of amino acids, the ErbB signaling pathway, the GnRH signaling pathway, the Toll-like receptor signaling pathway, cell adhesion molecules (CAMs), influenza A, and the MAPK signaling pathway (Fig. 2D).

Epitranscriptome-wide m⁶A modification analysis of circRNAs in Md5-infected CEF cells. To investigate the potential regulatory role of m⁶A on circRNAs, we carried out transcriptome-wide m⁶A modification profiling analysis. We detected 790 genes from a total of 932 annotated genes (the infected group) and 942 annotated genes (from the control group) in both the uninfected and Md5-infected CEF cells groups (Fig. 3A). We also detected 1199 from a total of 1483 and 1509 m⁶A modified peaks were in both the infected and control groups (Fig. 3B). m⁶A sites with a fold change (FC) > 2 were considered to be specific. Comparison of the infected group with control group revealed that 13% of the confirmed sites were specific to the infected group while 14% were specific to the control group. These results indicated that Md5 infection induced the reduction of the overall incidence of m⁶A modification in CEF cells.

To determine whether the m⁶A peak of circRNA featured a conserved RRACH sequence (in which the R represents purine, A represents m⁶A, and H is a non-guanine base). The sequences of the first 1000 peaks (50 bp on both sides of the peaks) with the largest enrichment factor in each group of samples were then selected and the sequences of these peaks were analyzed to identify meaningful motif sequences. We scanned part of the m⁶A modified peak sequence of the circRNA to determine whether the identified m⁶A peak contained the RRACH conservative motif sequence (where R represents purine, A represents m⁶A and H represents non-guanine bases). We found that GGAD (A, G, and U) GA was a reliable m⁶A modified motif in both the uninfected and Md5-infected groups obtained based on E-value (Fig. 3C).

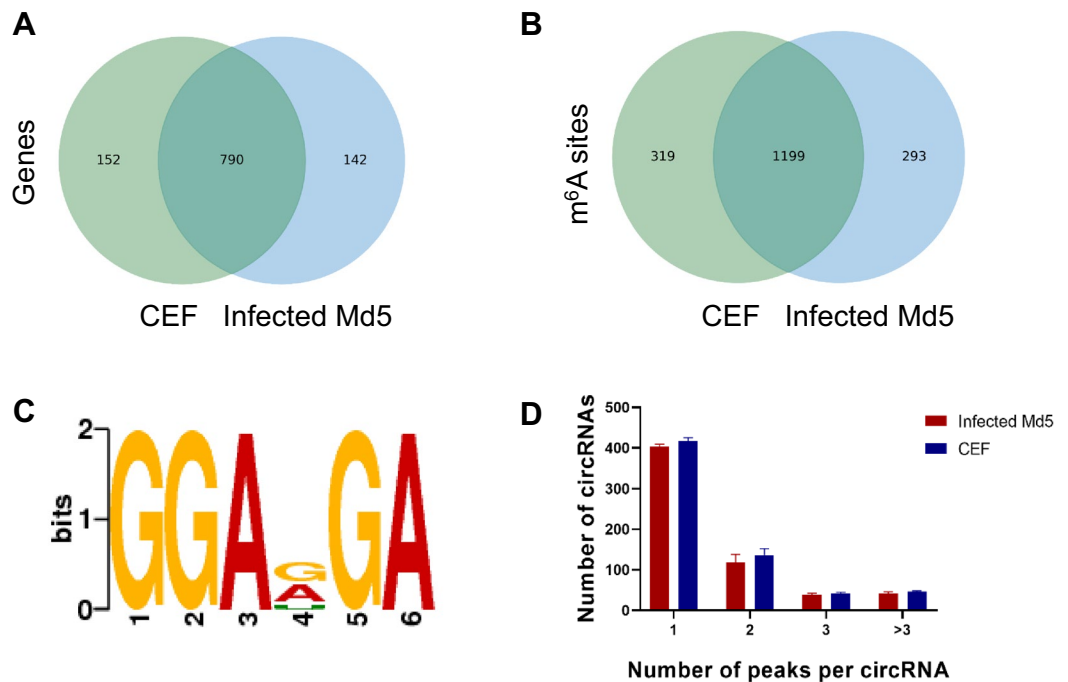


Figure 3. The characteristics of m⁶A peaks. (A) Venn diagram of m⁶A genes in infected Md5 and CEF groups; (B) Venn diagram of m⁶A methylation sites identified in circRNAs from infected and CEF groups; (C) The sequence motif of m⁶A sites in infected and control groups (Made by Discriminative Regular Expression Motif Elicitation (DREME), v5.3.3, <https://meme-suite.org/meme/tools/dreme>); (D) Proportion of genes harboring different numbers of m⁶A sites in the two groups (Made by Prism, v8.0.2, <https://www.graphpad.com>).

The m⁶A peak abundance of circRNA was further determined, the 67.1% of circRNAs in the infected group contained one m⁶A peak, slightly higher than the 65.0% of circRNAs in the control group. The numbers of two peaks (19.7% in the infected group vs. 21.2% in the control group), three peaks (6.3% in the infected group vs. 6.5% in the control group), and more than three peaks (6.9% in the infected group vs. 7.3% in the control group) were also determined (Fig. 3D), and the MAPK signaling pathway (Fig. 2D).

Heatmap of m⁶A levels of circRNAs in control and infected groups. Based on unsupervised hierarchical cluster analysis, there were significant differences in expression when compared between the infected and control groups (Fig. 4A). At the transcriptomic level, a total of 31 differentially expressed circRNAs were detected, among which 12 were up-regulated and 19 were down-regulated. Heatmaps of m⁶A methylation levels showed differences in expression between the infected and control groups (Fig. 4B). Of the 56 differentially expressed methylation modifications, 21 m⁶A modified peaks were detected in the up-regulated genes (Table 1) and 35 m⁶A modified peaks were detected in the down-regulated genes (Table 2). These results indicated that the different clustering could clearly distinguish the level of transcriptome-wide m⁶A modification between the Md5-infected and uninfected groups.

Chromosome visualization of m⁶A in circRNA. To investigate the distribution of m⁶A methylation sites within the entire genome, we scanned the m⁶A modified sites on all chromosomes. As an example, the methylation level and distribution of m⁶A on AKR1D1 gene differed when compared between the infected and control groups (Fig. 5). These results indicated the differential functions of m⁶A modification when compared between these two groups.

GO enrichment analysis of m⁶A in circRNAs. To examine the potential function of m⁶A modification in infected and control groups in vitro, we performed GO enrichment analysis. For BP, genes with up-regulated m⁶A sites were significantly enriched in organelle organization, cytoskeleton organization, actin filament-based process, actin cytoskeleton organization, peptidyl-amino acid modification, cytoskeleton organization, cell morphogenesis involved in differentiation, cell morphogenesis, actin filament-based process, and actin cytoskeleton organization (Fig. 6A). For cellular components (CC), genes with up-methylated m⁶A sites were mainly enriched in somatodendritic compartments, neuron projection, neuron part, dendrite cell projection, cell body, and axon; we did not detect the function of the methylated genes that were down-regulated (Fig. 6B). For MF, genes with up-regulated m⁶A sites were associated with transferase activity, transferring phosphorus-containing groups, signal transducer activity, receptor signaling protein activity, protein kinase activity, phosphotransferase activity, alcohol group as acceptor, molecular transducer activity, kinase activity, ATP binding, adenylyl ribonucleotide

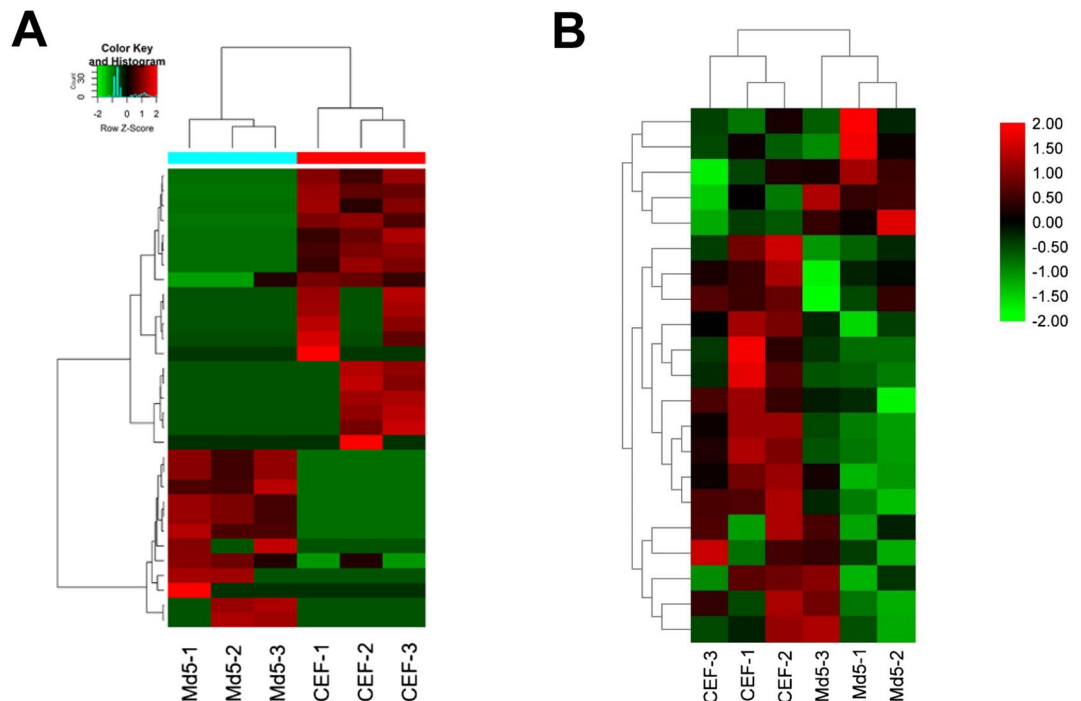


Figure 4. m⁶A modification clustering analysis. (A) Cluster analysis of m⁶A methylation at the transcriptome level. (B) Cluster analysis of m⁶A m⁶A modified lncRNA genes in the infected and control groups. The color represents the size of the log-fold enrichment (FE) value: the closer the color is to red, the larger the logFE value. Md5-1, Md5-2, Md5-3 represent the Md5-infected CEF group with three independent replicates. (Made by Tbttools, v1.082, <http://www.tbtools.org>).

chrom	txStart	txEnd	GeneName	Foldchange
1	32604598	32604680	-	128.7469112
1	91293301	91293320	ENSGALG00000024077	99.7
4	51575081	51575380	EPHA5	95.3
8	20814821	20815160	ARMH1	66.4
2	74540441	74540980	CDH18	60.7
5	42254121	42254360	FLRT2	14.30666667
2	1.07E+08	106671480	ENSGALG00000029474	12.02777778
1	1.77E+08	177137880	ENSGALG00000042343	9.117117117
2	2374581	2374900	GUK1	8.391304348
2	-	97042640	-	6.788732394

Table 1. Top ten up-methylated peaks of differentially m⁶A methylated sites in the infected group. “-” represents not available. Chrom: Chromosome; TxStart/TxEnd: Start/end position of the differentially methylated RNA peaks.

binding and adenyly nucleotide binding (Fig. 6C). With regards to BP and down-regulated genes, m⁶A sites were highly enriched in cellular carbohydrate metabolic process, regulation of carbohydrate metabolic process, positive regulation of carbohydrate metabolic process, monosaccharide biosynthetic process, hexose metabolic process, hexose biosynthetic process, glucose metabolic process, gluconeogenesis, cellular carbohydrate metabolic process and cell cycle G2/M phase transition (Fig. 6D). With regards to MF and downregulated genes, m⁶A sites were enriched in transferase activity, transferring acyl groups other than aminoacyl groups, transferase activity, transferring acyl groups, protein phosphatase binding, phosphatase binding, and enzyme inhibitor activity (Fig. 6E).

KEGG pathway analysis of m⁶A in circRNAs. The presence of m⁶A is critical to the normal function of cells. For each differentially expressed m⁶A modification site, we investigated the correlation with each up-regulated or down-regulated circRNA. To further explore the function of m⁶A in infected and control groups, we performed KEGG enrichment analysis of differentially m⁶A modified genes. The top 10 pathways included

chrom	txStart	txEnd	GeneName	Foldchange
1	4885621	4885840	PPARG	92.5
3	74518201	74518520	CDH18	71.9
19	83424141	83424380	CD200R1	65.7
21	19985261	19985480	PTPRF	22.3125
Z	8733401	8733640	ARPP19	20.34210526
13	30213841	30214120	IL15	10.22463768
2	16635161	16635420	ENSGALG00000029896	8.838095238
12	33409821	33410100	ENSGALG00000034760	7.806451613
2	24695481	24695720	SLC1A7	5.179153094
Z	11273981	11274180	-	5.04494382

Table 2. Top ten down-methylated peaks of differentially m⁶A methylated sites in the infected group. “-” represents not available. Chrom: Chromosome; TxStart/TxEnd: Start/end position of the differentially methylated RNA peaks.

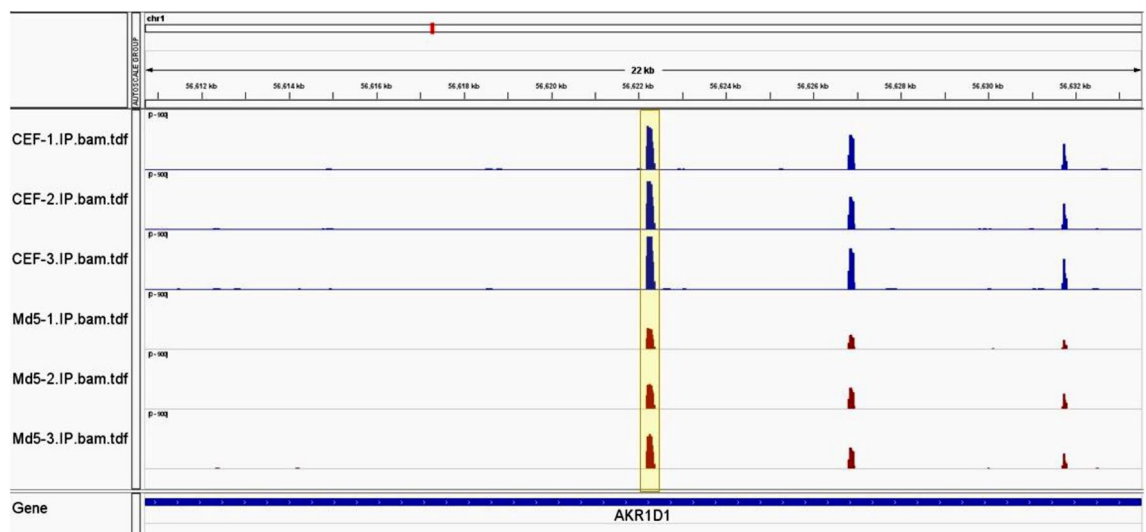


Figure 5. Chromosome visualization of m⁶A sites in lncRNAs. Red represents the infected group while blue represents the control group. Md5-1, Md5-2, Md5-3 represent the Md5-infected CEF group with three independent replicates. Differentially methylated m⁶A peaks visualized in Md5-infected group and control group. The highlighted area represents one of the differential methylation peaks.

progesterone-mediated oocyte maturation, dorsoventral axis formation, mTOR signaling pathway, ErbB signaling pathway, oocyte meiosis, vascular smooth muscle contraction, insulin signaling pathway, FoxO signaling pathway, purine metabolism, and regulation of actin cytoskeleton (Fig. 7A). The top 10 down-regulated pathways included primary bile acid biosynthesis, notch signaling pathway, PPAR signaling pathway, dorsoventral axis formation, immune network for IgA production, steroid hormone biosynthesis, adherens junction, TGF-beta signaling pathway, peroxisome and insulin resistance (Fig. 7B).

Discussion

Recent research identified 2169 circRNAs were discovered in the comprehensive analysis of differential expression profiling of the circRNA landscape in MDV-induced chicken tumorous spleens versus uninfected spleens¹². In the present study, we identified circRNAs that were differentially expressed in MDV-infected CEF cells. We found most of the circRNAs were produced from exonic, intronic, intergenic, sense overlapping, and antisense regions. Previous research has revealed that differentially expressed circRNAs are enriched in the apoptotic processes, nucleic acid binding region, DNA repair, and immune response during tumorigenesis¹². In MDV-infected CEF cells, however, genes related to chromosome segregation, carbohydrate binding, and glycosaminoglycan binding, were regulated. The differential expression profiling and function of circRNAs may be tissue- or tumorigenesis-specific. Furthermore, we investigated the differential expression profiling on m⁶A modified circRNAs. By measuring the degree of methylation in control and infected groups, we identified more than 1000 methylated peaks in circRNAs. We compared the sequences of the top ten peaks with the highest enrichment ratio of circRNA (50 bp on each side of the vertex). It was found that the GGAD (A, G, and U) GA sequence is one of the conserved motif sequences of circRNA based on E-value (Fig. 3C), which is different with canonical

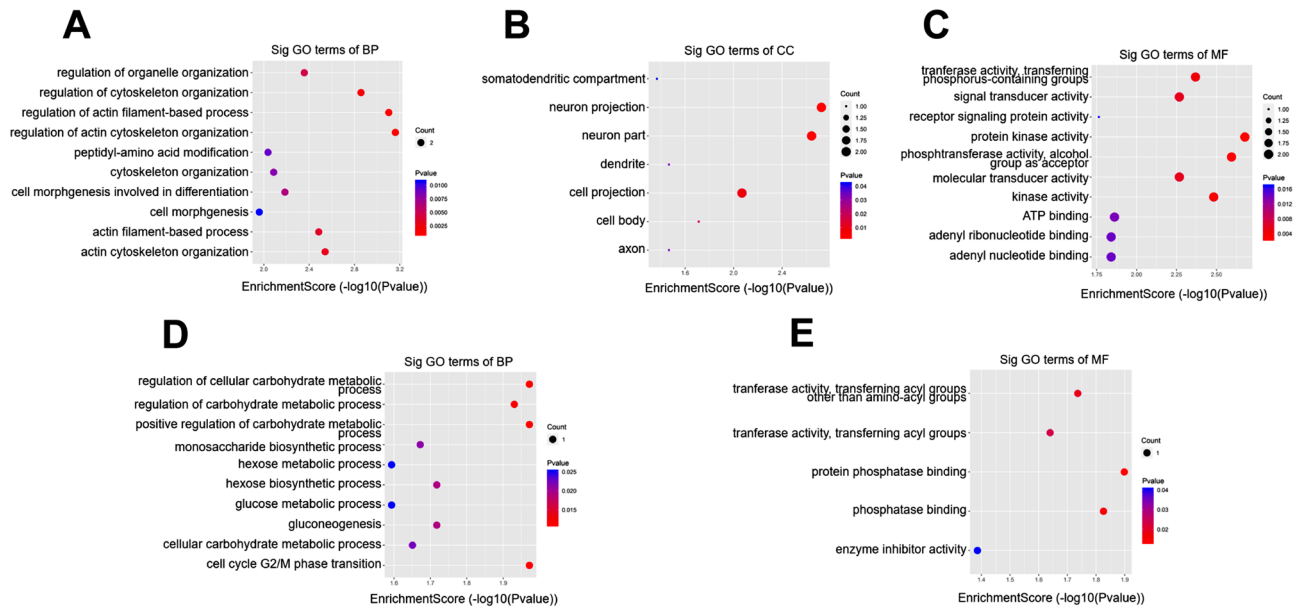


Figure 6. Gene ontology analyses of the infected and control groups. (A) The top ten gene ontology terms of biological processes were significantly enriched for the up-regulated genes; (B) The top seven gene ontology terms of cell component were significantly enriched for the up-regulated genes; (C) The top ten gene ontology terms of molecular functions were significantly enriched for the up-regulated genes; (D) The top ten gene ontology terms of biological process significantly enriched for down-regulated genes; (E) The top five gene ontology terms of molecular functions significantly enriched for down-regulated genes.

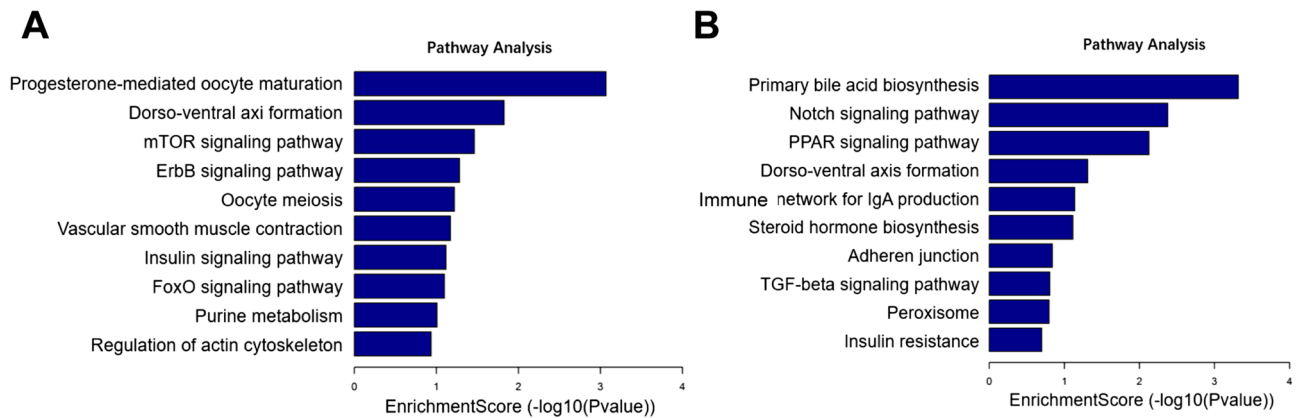


Figure 7. KEGG pathway analysis of differentially methylated m^6A genes in circRNAs. (A) Bar plot showing the top 10 enrichment scores of significantly enriched pathways for up-methylated m^6A genes in the infected group; (B) Bar plot showing the top 10 enrichment scores of significantly enriched pathways for down-methylated m^6A genes in the infected group.

DRACH/RRACH consensus motif sequence of m^6A deposition. Whether it is circRNA-specific motif sequence need to be further characterized.

Our results showed that the frequency of m^6A methylation and the number of methylated genes were slightly lower in the infected group than in the control group. However, our clustering analysis identified significant differences in the methylation levels of individual genes between the infected and control groups. Meanwhile, KEGG analysis identified the differential expression of circRNAs that were associated with specific signaling pathways in MDV-infected CEF cells. Interestingly, the ErbB signaling pathway induced by MDV infection was also regulated by m^6A modification. These data indicated the specific role of m^6A modified circRNAs in the replication of MDV in cultured CEF cells. In addition, the insulin signaling pathway was up-regulated while the insulin resistance signaling pathway was down-regulated. Previous research has demonstrated that insulin-like growth factor is abundantly expressed in MDV-mediated immune suppression and vaccine responses²⁷. Our results indicated that m^6A modification regulated the insulin signaling pathway and that this might be important in MDV infection and immune evasion. However, the specific mechanism by which m^6A modification acts on circRNA-associated signaling pathways has yet to be elucidated.

CircRNA can act as a miRNA sponge to affect gene expression in various biological and pathological activities^{28–30}. CircRNAs can bind with miR-155 in MDV-induced tumorous spleens; this is an orthologue of MDV-encoded MDV-miR-M4^{12,31}. Research has also shown that MDV-miR-M4 plays significant roles in tumorigenesis^{32,33}. In MDV-infected CEF cells, however, we did not identify a correlation between circRNAs and miRNAs, thus indicating that the m⁶A modification on circRNAs may change the regulatory role on miRNAs^{34,35}. It has also been demonstrated that miRNA can also be regulated by m⁶A modification. Whether m⁶A modified miRNA can affect gene expression in MDV infection needs to be further investigated.

It is of great important that we observed significantly higher expressions of METTL14 and ALBHK5 in MDV infected CEF cells comparing to uninfected control (Data not shown). These data suggest that MDV might change m⁶A modification of circRNAs through regulating activities of methyltransferase and demethylase to facilitate its replication and even pathogenesis. It is critical to know the detailed molecular mechanism of how MDV affect and regulate the circRNAs m⁶A modification in the next investigation. Meanwhile, the role of m⁶A modified circRNAs on MDV pathogenesis and even tumorigenesis also need to be further investigated.

Conclusions

We used MeRIP-sequencing to analyze circRNA m⁶A modifications in Md5-infected and uninfected control groups. We then compared the differences in m⁶A modification between the two groups. We identified the relative abundances of m⁶A modification and conserved motifs in MDV-infected and control groups. GO and KEGG analysis showed that up-regulated and down-regulated methylation genes were mainly associated with virus infection. However, the detailed regulatory role of m⁶A modified circRNAs in MDV infection needs to be investigated further.

Data availability

All data generated or analyzed during this study are included in this submitted manuscript. The datasets generated and/or analyzed during the current study are available in the NCBI repository (<https://www.ncbi.nlm.nih.gov/geo/>). The data is accessible via NCBI GEO submission ID: GSE166240. To review GEO accession GSE166240: Go to <https://www.ncbi.nlm.nih.gov/geo/query/acc.cgi?acc=GSE166240>. Enter token klufyeaed-nulxgb into the box.

Received: 1 February 2021; Accepted: 10 May 2021

Published online: 26 May 2021

References

- Biggs, P. M. & Nair, V. The long view: 40 years of Marek's disease research and Avian Pathology. *Avian Pathol.* **41**, 3–9. <https://doi.org/10.1080/03079457.2011.646238> (2012).
- Jarosinski, K. W., Tischer, B. K., Trapp, S. & Osterrieder, N. Marek's disease virus: lytic replication, oncogenesis and control. *Expert Rev Vaccines* **5**, 761–772. <https://doi.org/10.1586/14760584.5.6.761> (2006).
- Calnek, B. W. Pathogenesis of Marek's disease virus infection. *Curr. Top. Microbiol. Immunol.* **255**, 25–55. https://doi.org/10.1007/978-3-642-56863-3_2 (2001).
- Schumacher, D., Tischer, B. K., Fuchs, W. & Osterrieder, N. Reconstitution of Marek's disease virus serotype 1 (MDV-1) from DNA cloned as a bacterial artificial chromosome and characterization of a glycoprotein B-negative MDV-1 mutant. *J. Virol.* **74**, 11088–11098. <https://doi.org/10.1128/jvi.74.23.11088-11098.2000> (2000).
- Lee, L. F. *et al.* The complete unique long sequence and the overall genomic organization of the GA strain of Marek's disease virus. *Proc. Natl. Acad. Sci. U S A* **97**, 6091–6096. <https://doi.org/10.1073/pnas.97.11.6091> (2000).
- Osterrieder, N., Kamil, J. P., Schumacher, D., Tischer, B. K. & Trapp, S. Marek's disease virus: from miasma to model. *Nat. Rev. Microbiol.* **4**, 283–294. <https://doi.org/10.1038/nrmicro1382> (2006).
- Esteller, M. Non-coding RNAs in human disease. *Nat. Rev. Genet.* **12**, 861–874. <https://doi.org/10.1038/nrg3074> (2011).
- Vicens, Q. & Westhof, E. Biogenesis of circular RNAs. *Cell* **159**, 13–14. <https://doi.org/10.1016/j.cell.2014.09.005> (2014).
- Dou, C. *et al.* Changing expression profiles of lncRNAs, mRNAs, circRNAs and miRNAs during osteoclastogenesis. *Sci. Rep.* **6**, 21499. <https://doi.org/10.1038/srep21499> (2016).
- Militello, G. *et al.* Screening and validation of lncRNAs and circRNAs as miRNA sponges. *Brief Bioinform.* **18**, 780–788. <https://doi.org/10.1093/bib/bbw053> (2017).
- Zhang, X. *et al.* Circular RNA alterations are involved in resistance to avian leukosis virus subgroup-J-induced tumor formation in chickens. *Oncotarget* **8**, 34961–34970. <https://doi.org/10.18632/oncotarget.16442> (2017).
- Wang, L. *et al.* Genome-wide analysis of circular RNAs involved in Marek's disease tumorigenesis in chickens. *RNA Biol.* **17**, 517–527. <https://doi.org/10.1080/15476286.2020.1713538> (2020).
- Qiu, L., Chang, G., Bi, Y., Liu, X. & Chen, G. Circular RNA and mRNA profiling reveal competing endogenous RNA networks during avian leukosis virus, subgroup J-induced tumorigenesis in chickens. *PLoS ONE* **13**, e0204931. <https://doi.org/10.1371/journal.pone.0204931> (2018).
- Tsai, K. & Cullen, B. R. Epigenetic and epitranscriptomic regulation of viral replication. *Nat. Rev. Microbiol.* **18**, 559–570. <https://doi.org/10.1038/s41579-020-0382-3> (2020).
- Yu, J. *et al.* Dynamic m⁶A modification regulates local translation of mRNA in axons. *Nucl. Acids Res.* **46**, 1412–1423. <https://doi.org/10.1093/nar/gkx1182> (2018).
- Dai, D., Wang, H., Zhu, L., Jin, H. & Wang, X. N⁶-methyladenosine links RNA metabolism to cancer progression. *Cell Death Dis.* **9**, 124. <https://doi.org/10.1038/s41419-017-0129-x> (2018).
- Wang, X. *et al.* Structural basis of N(6)-adenosine methylation by the METTL3-METTL14 complex. *Nature* **534**, 575–578. <https://doi.org/10.1038/nature18298> (2016).
- Peters, T., Ausmeier, K. & Ruther, U. Cloning of Fatso (Fto), a novel gene deleted by the Fused toes (Ft) mouse mutation. *Mamm. Genome* **10**, 983–986. <https://doi.org/10.1007/s003359901144> (1999).
- Gerken, T. *et al.* The obesity-associated FTO gene encodes a 2-oxoglutarate-dependent nucleic acid demethylase. *Science* **318**, 1469–1472. <https://doi.org/10.1126/science.1151710> (2007).
- Jia, G. *et al.* N⁶-methyladenosine in nuclear RNA is a major substrate of the obesity-associated FTO. *Nat. Chem. Biol.* **7**, 885–887. <https://doi.org/10.1038/nchembio.687> (2011).

21. Chen, M. N. & Wong, C. M. The emerging roles of N6-methyladenosine (m6A) deregulation in liver carcinogenesis. *Mol. Cancer* **19**, 44. <https://doi.org/10.1186/s12943-020-01172-y> (2020).
22. Zhou, C. *et al.* Genome-wide maps of m6A circRNAs identify widespread and cell-type-specific methylation patterns that are distinct from mRNAs. *Cell Rep.* **20**, 2262–2276. <https://doi.org/10.1016/j.celrep.2017.08.027> (2017).
23. Asada, K. *et al.* Critical roles of N(6)-methyladenosine (m(6)A) in cancer and virus infection. *Biomolecules* **10**, 1071. <https://doi.org/10.3390/biom10071071> (2020).
24. Sun, A. J. *et al.* Lorf9 deletion significantly eliminated lymphoid organ atrophy induced by meq-deleted very virulent Marek's disease virus. *Vet. Microbiol.* **235**, 164–169 (2019).
25. Meyer, K. D. *et al.* Comprehensive analysis of mRNA methylation reveals enrichment in 3' UTRs and near stop codons. *Cell* **149**, 1635–1646. <https://doi.org/10.1016/j.cell.2012.05.003> (2012).
26. Kanehisa, M. & Goto, S. KEGG: kyoto encyclopedia of genes and genomes. *Nucl. Acids Res.* **28**, 27–30. <https://doi.org/10.1093/nar/28.1.27> (2000).
27. Neerukonda, S. N., Tavlarides-Hontz, P., McCarthy, F., Pendarvis, K. & Parcels, M. S. Comparison of the transcriptomes and proteomes of serum exosomes from marek's disease virus-vaccinated and protected and lymphoma-bearing chickens. *Genes* **10**, 116. <https://doi.org/10.3390/genes10020116> (2019).
28. Nahand, J. S. *et al.* Circular RNAs: new epigenetic signatures in viral infections. *Front. Microbiol.* **11**, 1853. <https://doi.org/10.3389/fmicb.2020.01853> (2020).
29. Zhang, X. *et al.* Circular RNA Vav3 sponges gga-miR-375 to promote epithelial-mesenchymal transition. *RNA Biol.* **16**, 118–132. <https://doi.org/10.1080/15476286.2018.1564462> (2019).
30. Dori, M. & Biccato, S. Integration of bioinformatic predictions and experimental data to identify circRNA-miRNA associations. *Genes* **10**, 642. <https://doi.org/10.3390/genes10090642> (2019).
31. Zhao, Y. *et al.* A functional MicroRNA-155 ortholog encoded by the oncogenic Marek's disease virus. *J. Virol.* **83**, 489–492. <https://doi.org/10.1128/JVI.01166-08> (2009).
32. Zhao, Y. *et al.* Critical role of the virus-encoded microRNA-155 ortholog in the induction of Marek's disease lymphomas. *PLoS Pathog.* **7**, e1001305. <https://doi.org/10.1371/journal.ppat.1001305> (2011).
33. Zhuang, G. Q., Sun, A. J., Teng, M. & Luo, J. A tiny RNA that packs a big punch: the critical role of a viral miR-155 Ortholog in lymphomagenesis in marek's disease. *Front. Microbiol.* **8**, 1169. <https://doi.org/10.3389/fmicb.2017.01169> (2017).
34. Tang, Y. *et al.* m6A-Atlas: a comprehensive knowledgebase for unraveling the N6-methyladenosine (m6A) epitranscriptome. *Nucl. Acids Res.* **49**(D1), D134–D143. <https://doi.org/10.1093/nar/gkaa692> (2020).
35. Fazi, F. & Fatica, A. Interplay between N(6)-methyladenosine (m(6)a) and non-coding rnas in cell development and cancer. *Front Cell Dev. Biol.* **7**, 116. <https://doi.org/10.3389/fcell.2019.00116> (2019).

Acknowledgements

We would like to thank Dr. Zhizhong Cui (Professor of Virology in Shandong Agricultural University) for providing Md5 strain of MDV.

Author contributions

Conceptualization, G.Q.Z. and A.S.; methodology, R.W. and S.Y.; software, X.Z.; validation, Y.L., M.T. and L.Z.; formal analysis, J.L.; data curation, R.W.; writing—original draft preparation, G.Q.Z.; writing—review and editing, G.Q.Z. and A.S.; supervision, G.Q.Z. and G.P.Z.; project administration, G.Q.Z. and G.P.Z.; funding acquisition, G.Q.Z., J.L. and A.S. All authors have read and agreed to the published version of the manuscript.

Funding

This work is supported by Grants of the Starting Foundation for Outstanding Young Scientists of Henan Agricultural University (No 30500690); Advanced program of 2020 for returned overseas scholar (No 30602136); The grants of National Natural Science Foundation of China (No 31802160 and U1604232); The Henan Thousand Talents Program-Leading Talents in Basic Research (2019–2020); The Natural Science Foundation of Henan Province (2021); and The Key R&D and Promotion Project of Henan Province (2021). The grants above were used in the design of the study and collection, analysis, and interpretation of data and in writing the manuscript.

Competing interests

The authors declare no competing interests.

Additional information

Correspondence and requests for materials should be addressed to G.Z.

Reprints and permissions information is available at www.nature.com/reprints.

Publisher's note Springer Nature remains neutral with regard to jurisdictional claims in published maps and institutional affiliations.



Open Access This article is licensed under a Creative Commons Attribution 4.0 International License, which permits use, sharing, adaptation, distribution and reproduction in any medium or format, as long as you give appropriate credit to the original author(s) and the source, provide a link to the Creative Commons licence, and indicate if changes were made. The images or other third party material in this article are included in the article's Creative Commons licence, unless indicated otherwise in a credit line to the material. If material is not included in the article's Creative Commons licence and your intended use is not permitted by statutory regulation or exceeds the permitted use, you will need to obtain permission directly from the copyright holder. To view a copy of this licence, visit <http://creativecommons.org/licenses/by/4.0/>.

© The Author(s) 2021